Heliyon 10 (2024) e36848

Contents lists available at ScienceDirect

Heliyon

journal homepage: www.cell.com/heliyon

Research article

Efficient removal of chlortetracycline hydrochloride and doxycycline hydrochloride from aqueous solution by ZIF-67

Ke Li, Miaomiao Chen, Lei Chen *, Songying Zhao, Wenbo Pan, Pan Li

Key Laboratory of Songliao Aquatic Environment, Ministry of Education, Jilin Jianzhu University, Changchun, 130118, China

ARTICLE INFO

Keywords:
ZIF-67
Adsorption
Chlortetracycline hydrochloride
Doxycycline hydrochloride

ABSTRACT

ZIF-67 nanoparticles were synthesized by a simple method at room temperature and used to remove chlortetracycline hydrochloride (CTC) and doxycycline hydrochloride (DOX) from water. ZIF-67 was characterized by scanning electron microscopy (SEM), transmission electron microscopy (TEM), fourier transform infrared spectroscopy (FT-IR), Brunauer-Emmett-Teller (BET) surface area, X-ray photoelectron spectroscopy (XPS), thermogravimetry (TGA) and zeta potential analyzer. The morphology and chemical composition of the synthesized ZIF-67 were characterized. The effects of key parameters such as pH, dosage, temperature, contact time, different initial concentrations and coexisting ions on the adsorption behavior were systematically studied. The results of batch adsorption experiments indicate that the adsorption process conforms to the pseudo-second-order kinetic model and Sips model. At 303K, the removal rates of CTC and DOX at 150 mg/L reached 99.16 % and 97.61 %, and the maximum adsorption capacity of CTC and DOX reached 1411.68 and 1073.28 mg/g, respectively. At the same time, ZIF-67 has excellent stability and reusability. Most importantly, the possible adsorption mechanism is proposed by exploring the changes of SEM, TEM, BET and FT-IR characterization results before and after the reaction, which mainly includes pore filling, electrostatic interaction and π-π interaction. The prepared ZIF-67 has a large specific surface area (1495.967 $m^2 g^{-1}$), achieves a high removal rate within a short time frame, and maintains a high removal rate across a wide pH range. These characteristics make ZIF-67 a potentially promising adsorbent for removing antibiotics from aqueous solutions.

1. Introduction

In recent years, the issue of water pollution has emerged as a serious problem facing the whole world particularly antibiotics, are among the persistent pollutants that have received widespread attention [1]. The discovery of antibiotic treatment was a significant medical breakthrough of the 20th century. However, due to their low cost and excessive use, antibiotics are now pervasively present in the biological chain [2], which seriously affects the health of humans and animals. Furthermore, antibiotics have been detected in sewage treatment plants and natural water [3,4], thereby posing a serious threat to the living environment of humans and animals. Among all kinds of antibiotics, tetracycline antibiotics are the second most produced and used in the world, and due to their chemical nature, most antibiotics can be protonated/deprotonated at different pH, leading to their widespread presence in diverse environments

* Corresponding author.
E-mail addresses: like123@163.com (K. Li), chenm192@163.com (M. Chen), chenlei.jliae@hotmail.com (L. Chen), zhaosongying1980@sina.com (S. Zhao), panwenbo2023@163.com (W. Pan), lipan990811@163.com (P. Li).

https://doi.org/10.1016/j.heliyon.2024.e36848
Received 19 May 2024; Received in revised form 14 August 2024; Accepted 22 August 2024

[5,6]. Specifically, CTC and DOX are inexpensive tetracycline antibiotics that are widely used in modern society to prevent bacterial growth and protein synthesis [7–9]. Tetracycline antibiotics have also been reported as toxic hazards to humans, such as acute pancreatitis, fatty liver, bilirubin, elevated triglycerides, etc [10]. Therefore, it is necessary to develop efficient and economically feasible methods to remove antibiotics from water.

Currently, various methods are employed to remove antibiotics from water. The main methods of removing antibiotics from water are adsorption [11–16], photocatalysis [17–21], electrochemical method [22], biodegradation method [23,24], ozonation technique [25], membrane separation [26] and others. Among these, adsorption is considered to be one of the most effective methods for removing antibiotics from water, owing to its economical, efficient, simple operation and high repeatability [3,27–32]. A variety of adsorbent materials are used as adsorbents for antibiotics [6,33–36]. For instance, Hao et al. [37] used nanocomposites of zero-valent iron@biochar removed oxytetracycline, chlortetracycline and tetracycline from the water with adsorption capacities of 52.7, 42.5 and 39.1 mg/g, respectively. Egbedina et al. [38] utilized CTAB-activated Carbon from Peanut Husks to remove tetracycline and amoxicillin from water with a maximum adsorption capacity of 272 and 305 mg/g, respectively. However, these adsorbents often come with limitations such as low adsorption removal rates and complex synthesis methods, underscoring the urgent need for adsorbents with high efficiency and simple synthesis approaches.

Metal-organic frameworks (MOFs), an emerging kind of porous material, are composed of crystalline materials that are self-assembled by metal ions or metal clusters and organic ligands [3]. Hundreds of different MOFs have been developed for applications in the fields of gas separation, gas storage, energy storage, adsorption and catalysis [39–41]. Due to its large specific surface area [33,42], large pore volume [43], adjustable [44,45] and easy functionalization [46], these characteristics make it widely used in the field of adsorbing antibiotics. ZIF-67 is one of the most widely studied materials in the MOFs family and has been used in the field of adsorption. Lin et al. [47] used ZIF-67 to remove malachite green (MG) from water, showcasing an extremely high adsorption capacity of 2430 mg/g at 20 °C, which is attributed to the π-π interaction between MG and ZIF-67. Nevertheless, literature on the removal of CTC and DOX using ZIF-67 remains scarce.

In this work, ZIF-67 was synthesized through a straightforward method and applied for the removal of CTC and DOX in water. By investigating parameters, optimal experimental conditions were established and applied to batch experiments. A variety of characterization methods including SEM, TEM, BET, FT-IR, XRD, XPS and TGA were then used to understand the properties of ZIF-67. At the same time, adsorption kinetics and adsorption isotherm were used to elucidate the adsorption process.

2. Materials and methods

2.1. Materials and regants

Cobalt nitrate hexahydrate ($Co(NO_3)_2{\cdot}6H_2O$, 99 %) and 2-Methylimidazole ($C_4H_6N_2$, 98 %) were acquired from Shanghai Macklin Biochemical Co., Ltd. Methanol (CH_3OH, AR) was sourced from Tianjin Xinbote Chemical Co., Ltd. Absolute ethanol (C_2H_5OH, AR) were obtained from Tianjin Jindong Tianzheng Fine Chemical Reagent Factory. CTC ($C_{22}H_{23}ClN_2O_8{\cdot}HCl$, 99.9 %) and DOX ($C_{22}H_{24}N_2O_8{\cdot}HCl$, 98 %) were supplied by Shanghai yuanye Bio-Technology Co., Ltd. All chemicals were used as received without further purification. Deionized (DI) water produced in the laboratory was used throughout the experiments.

2.2. Synthesis of ZIF-67

ZIF-67 was synthesized according to the method already reported with some modifications [48]. Firstly, 1.35g cobalt nitrate hexahydrate was dissolved in 9 mL deionized (DI) water. Subsequently, 16.5g 2-methylimidazole was dissolved in another beeker containing 60 mL of DI water. The two solutions were mixed and stirred continuously at room temperature for 6h. The resulting purple

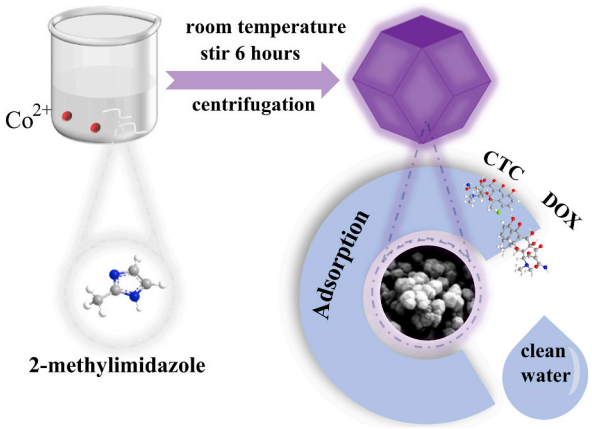

Fig. 1. Synthesize ZIF-67 flow chart.

solution was centrifuged, the collected purple precipitate was then washed several times with methanol, and finally dried overnight at 80 °C. The synthesis process is shown in Fig. 1.

2.3. Adsorption experiments

Batch adsorption experiments were conducted to analyze the adsorption capacity of ZIF-67. Specifically, 10 mg of ZIF-67 was dispersed in 20 mL of CTC and DOX solutions, respectively. Both antibiotics were dissolved in DI water to prepare a stock solution of 1500 mg/L, which was then diluted as needed. In the batch adsorption experiment, 150 mg/L CTC and DOX were used to investigate. In the pH influence experiment, NaOH and HCl were used to adjust the concentration of CTC and DOX to 3–11, the contact time was carried out within 240min, and the effect of dosage was 0.1–0.9 g/L for the experiment. The adsorption isotherm model was analyzed at different initial concentrations (100–1300 mg/L), and the adsorption kinetics model was analyzed at 100–200 mg/L The experiments were carried out in a thermoshaker set to a predetermined temperature and agitated at 150 rpm to prevent any limitation due to liquid-to-solid transfer. After the adsorption experiment, the solution was filtered through a 0.22 μm membrane. The residual concentrations of CTC and DOX were determined by UV–VIS spectrophotometry. All experiments were repeated three times. The equilibrium adsorption capcity and removal efficiency of ZIF-67 for antibiotics were calculated using Eqs. (1) and (2), respectively.

$$q_e = \frac{C_0 - C_e}{m} \times v \tag{1}$$

$$R(\%) = \frac{C_0 - C_e}{C_0} \times 100 \tag{2}$$

where, q_e (mg g^{-1}) is the equilibrium adsorption capacity that reaches equilibrium, C_0 (mg L^{-1}) is the initial concentration of the antibiotic, C_e (mg L^{-1}) is the remaining concentration when reaching equilibrium, m (g) is the mass of the adsorbent added, and v (L) is the volume of the antibiotic.

2.4. Regeneration and reusability

After the adsorption experiment, ZIF-67 crystals were collected, and washed with ethanol for several times, then collected again. After drying, the crystals were stored for subsequent experimental cycles.

2.5. Characterization technique

The synthetic samples were characterized and analyzed by various characterization techniques. The crystal phase of the obtained sample was characterized by XRD and scanning 2θ range 5–40°. The morphology of the samples was detected by SEM (ZEISS,

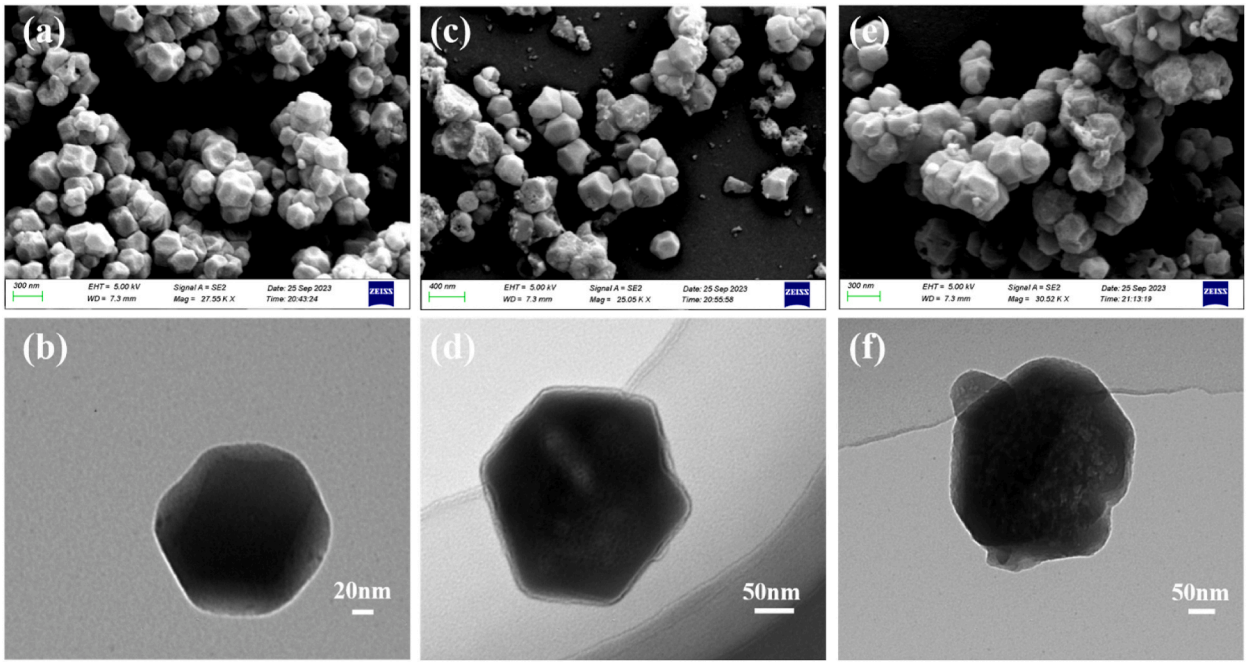

Fig. 2. SEM and TEM of ZIF-67 (a) and (b), after CTC (c) and (d), after DOX (e) and (f).

Germany) and TEM (Hitachi, Japan). The presence of various special functional groups in the samples was verified by FT-IR (PerkinElmer, USA). The N_2 adsorption-desorption isotherms (Quantachrome, USA) experiments were performed, which helped determine the BET surface area and pore size distribution of the sample. The surface element composition and chemical state of the material were studied by XPS (Thermo, USA). The Nano ZS90 nm Particle Size Meter (Malvern, UK) provided zeta potential measurement. The thermal properties of ZIF-67 were analyzed by TGA. T6 spectrophotometer (Beijing, China) was used to determine the concentration of CTC and DOX solution and PHBJ-260 instrument (Shanghai, China) was used to determine the pH of the solution.

3. Results and discussion

3.1. Characterization of the ZIF-67

The morphology of ZIF-67, both before and after the reaction, was thoroughly examined by SEM and TEM, with the findings illustrated in Fig. 2. As can be seen from Fig. 2(a) and (b), the synthesized material has smooth outer surface and uniform size in 150–300 nm, and a typical rhombohedral morphology. These characteristics align closely with those reported in previous studies [49,50]. Fig. 2(c–f) reveal that the morphology of the nanocrystals after the reaction with CTC and DOX does not change significantly. Compared with (a), the surface of (c) (e) is rougher. Furthermore, TEM images post-reaction highlight that the edges of the ZIF-67 crystals appear blurred, and a coating of contaminants is visible, signifying the adsorption of contaminants onto the ZIF-67 nanoparticles. In addition, TEM images after the reaction showed that the crystal edges of ZIF-67 became blurred and could be seen to be coated with contaminants, indicating that contaminants were adsorbed on the ZIF-67 nanoparticles.

The XRD pattern of ZIF-67 crystal, before and after the reaction, is presented in Fig. 3 (a). The XRD pattern confirms the crystal structure of the synthesized material. Fig. 3 (a) shows that the characteristic peaks are located at 7.3° (011), 10.3° (002), 12.7° (112), 14.6° (022), 16.4° (013), 18.0° (222), 22.1° (114), 24.5° (233), 25.6° (224), 26.6° (134), 29.6° (044), 30.5° (334), 31.4° (244), 32.3° (235) [47,51]. After the reaction, the strength of the characteristic peak of the material is obviously reduced, and the original characteristic structure of ZIF-67 crystal is maintained. This reduction in peak intensity and slight shift in their positions, due to the adsorption of CTC and DOX, suggests that the material's structure remains stable, marking it as a promising candidate for further applications. Due to the adsorption of CTC and DOX, the intensity of characteristic peaks decreased significantly and their positions shifted slightly. It shows that the structure of the material is stable and it is a promising material for removing both antibiotics. The functional groups of the adsorbent before and after the reaction were analyzed by FT-IR. As illustrated in Fig. 3 (b), the sharp peak of the adsorbent at 425 cm^{-1} corresponds to the Co-N bond vibration of ZIF-67, indicating a successful connection between Co and N in 2-methylimidazole [52,53]. The characteristic peaks at 600-1500 cm^{-1} are caused by the stretching and bending patterns of imidazole rings [47,51,54]. Additionally, the peak at 1632 cm^{-1} is identified as the C=N band, and peak at 1457 cm^{-1} is related to the C=C of the imidazole group [55]. The absorption peaks at 2925 cm^{-1} and 3134 cm^{-1} are influenced by the C-H bands on the methyl and imidazole rings, respectively. The wide band at 3435 cm^{-1} can be attributed to the stretching vibration of the -OH group [56,57]. The infrared spectrum after the reaction of adsorbents and antibiotics is shown in Fig. 3 (b), which functional group changes can be observed. After the reaction of ZIF-67 with CTC, the main functional groups did not change significantly, indicating the stability of the material. A new characteristic peak appeared at 1049 and 1090 cm^{-1}, indicating that C-O functional groups were bound to the surface of the adsorbent [58]. In addition, a new peak was observed at 1598 cm^{-1} and 1596 cm^{-1}, and a peak enhancement at 1415 cm^{-1}, which are attributed to the stretching vibration of the C=C bond in the antibiotic [59], confirming the presence of CTC and DOX in ZIF-67.

The structural characteristics of the prepared samples were investigated by the N_2 adsorption-desorption isotherms (Fig. 3 (c) (d)). It can be observed from Fig. 3 (c) that the adsorption capacity of the prepared sample increases sharply under low pressure and then increases slowly. This is a typical feature of a type I adsorption isotherm, which indicates the presence of microporous materials [54]. As proved in Fig. 3 (d) that ZIF-67 mainly has microporous and mesoporous structures. The specific surface area and pore characteristics of the synthetic materials before and after the reaction are summarized in Table 1. The prepared ZIF-67 has a high specific surface area (1495.967 $m^2\ g^{-1}$), the specific surface area and pore volume of ZIF-67 after the reaction were investigated, and it was

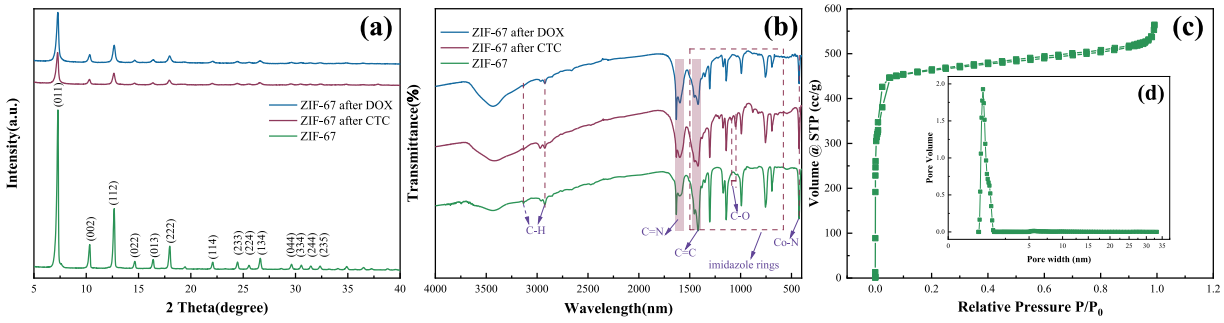

Fig. 3. ZIF-67 before and after reaction (a) XRD; (b) FTIR; (c) N_2 adsorption-desorption isotherms of ZIF-67; (d) pore size distribution curves of ZIF-67.

found that the changes were reduced, which indicated that the pores in ZIF-67 were blocked during the reaction [60]. This implies that the pore-filling effect may also enhance the adsorption process. It can be inferred from the above that the pore filling effect may also have a certain promoting effect in the adsorption process.

To delve into the chemical state ZIF-67, XPS was performed. Fig. 4(a–e) displays the XPS spectra of ZIF-67, including the full spectrum and individual spectra for C, N, O, and Co elements. In Fig. 4 (a), peaks corresponding to Co2p, O1s, N1s, and C1s can be observed, and consistent with the reported literature [61]. The Co2p spectra, shown in Fig. 4 (b), can be deconvoluted into four peaks. The peaks at 781.7 eV and 797.2 eV are attributed to Co^{3+}, while those at 788.5 eV and 804.1 eV belong to Co^{2+}. Specifically, the binding energy of 781.7eV and 788.5eV correspond to $Co2p_{3/2}$, while 797.2eV and 804.1eV belong to $Co2p_{1/2}$ [54,62]. The O1s spectrum primarily exhibits two peaks. The peak at 531.97eV is assigned to C-O bonds, while the peak at 533.1eV corresponds to, O-H/C-O-C groups [63]. In the C1s spectrum, peaks at 284.65, 286.05 and 288.62eV represent the C=C/C-C, C=N/C-N and C=O functional groups, respectively [64]. Finally, the N1s spectrum shows two characteristic peaks at 398.75 and 400.2eV, corresponding to C-N and C=N bonds, respectively [63].

The thermal stability of ZIF-67 was analyzed by TGA detection technique in N_2 atmosphere, and the resulting TGA curve is presented in Fig. 4 (f). It can be observed from the figure that the weight loss curve of ZIF-67 has two main weight loss peaks, which is similar to the literature [65]. ZIF-67 demonstrates good thermal stability below 260 °C. The mass loss of approximately 25 % observed at 260–480 °C is primarily attributed to the decomposition of solvents and small molecules [66]. The 47 % mass loss at 480–670 °C is mainly due to the collapse of the ZIF-67 structure as the material begins to decompose [67]. These results confirm the good thermal stability of ZIF-67.

3.2. Bath experimentals

3.2.1. Effect of pH

The pH value of the solution is an important factor affecting the adsorption effect of the adsorbent. It plays a crucial role in the whole experiment. To investigate this, 150 mg/L CTC and DOX solutions with pH range of 3–11 were used to explore the influence on adsorption efficiency, and Fig. 5 (a) depicts the experimental results. Fig. 5 (a) despits that ZIF-67 is prominent for both CTC and DOX removal capacity over a broad pH value. Fig. 5(b) demonstrates the zeta potential of ZIF-67 at different pH conditions, and it is concluded that the zero point occurs at $pH_{pzc} = 10.6$. When the pH of ZIF-67 is less than 10.6, the material surface is positively charged, and when the pH of ZIF-67 is greater than 10.6, the material surface is negatively charged. For CTC, when pH is 3–4, the removal rate increases slowly, the highest removal rate appears at pH = 4 (99.16 %), and gradually decreases at pH = 5–11. Within the pH value of 3–9, the removal rate is all above 90 %. For DOX, when pH = 3–8, it shows an upward trend, the highest removal rate appears at pH = 8 (97.61 %), and then slowly decreases at 9–11, the removal rate exceeds 95 % within the pH value of 3–10. The morphology of CTC and DOX in aqueous solution changes with pH value. CTC has three acid dissociation constants ($pK_{a1} = 3.33$, $pK_{a2} = 7.55$, $pK_{a3} = 9.33$), and CTC is mainly divided into four types: $CTCH_3^+$ (pH < 3.3), $CTCH_2^{\pm}$(3.3<pH < 7.5), $CTCH^-$ (7.5 < pH < 9.3), and CTC^{2-} (pH > 9.3) [58]. Similarly, there are three acid dissociation constants for DOX, which are $pK_{a1} = 3.5$, $pK_{a2} = 7.7$, $pK_{a3} = 9.5$ [11]. And the main four molecular structure of DOX at different pH values: DOX^+ (pH < 3.5), DOX^-(3.5<pH < 7.7), DOX^0 (7.7<pH < 9.5), DOX^{2-} (pH > 9.5). When pH = 3, CTC and DOX solution are positively charged, and the adsorbent surface is negatively charged, so the adsorption effect is slightly lower. When pH = 4–7, the surface of CTC becomes neutral, the surface of DOX becomes negative, and the removal rate is enhanced due to electrostatic interaction. Similarly, when pH = 8–9, the surface of DOX becomes neutral, the surface of CTC becomes negative, and the removal rate is enhanced due to electrostatic interaction. At pH = 11, both the adsorbents and antibiotics carry a negative charge, resulting in increased electrostatic repulsion a consequent drop in removal efficiency. According to zeta potential analysis, the highest charge removal efficiency is anticipated at pH 10. This indicates that the strong electrostatic interaction plays an important role in the adsorption of CTC and DOX by the prepared adsorbents, but it cannot be attributed only to the electrostatic interaction. Therein, both CTC/DOX and ZIF-67 contain aromatic ring structure, it is possible that the aromatic structure in CTC and DOX interacts with the π-π interaction in the benzene ring in ZIF-67. As can be seen from the above, in addition to electron interaction, π-π interaction may also controls the adsorption reaction process.

3.2.2. Effect of dosage

Fig. 5 (c) displays the effects of different dosing amounts of adsorbents on the removal rates of CTC and DOX. With the dosing rate increasing from 0.1 to 0.9 g/L, the removal rates of CTC and DOX increased from 98.34 % and 95.97 % to 99.25 % and 98.19 %, respectively. This can be attributed to the increase of active sites on the surface of the adsorbent, allowing more pollutant molecules to be adsorbed on the adsorbent surface. The balance was maintained at 0.5–0.9 g/L, so 0.5 g/L was chosen as the dosage for subsequent experiments.

Table 1
Structural characteristics of ZIF-67.

Sample	BET surface area ($m^2\ g^{-1}$)	Pore volume (cc g^{-1})	Pore width (nm)
ZIF-67	1495.967	0.752	0.926
After CTC	916.249	0.632	0.852
After DOX	1001.630	0.636	0.926

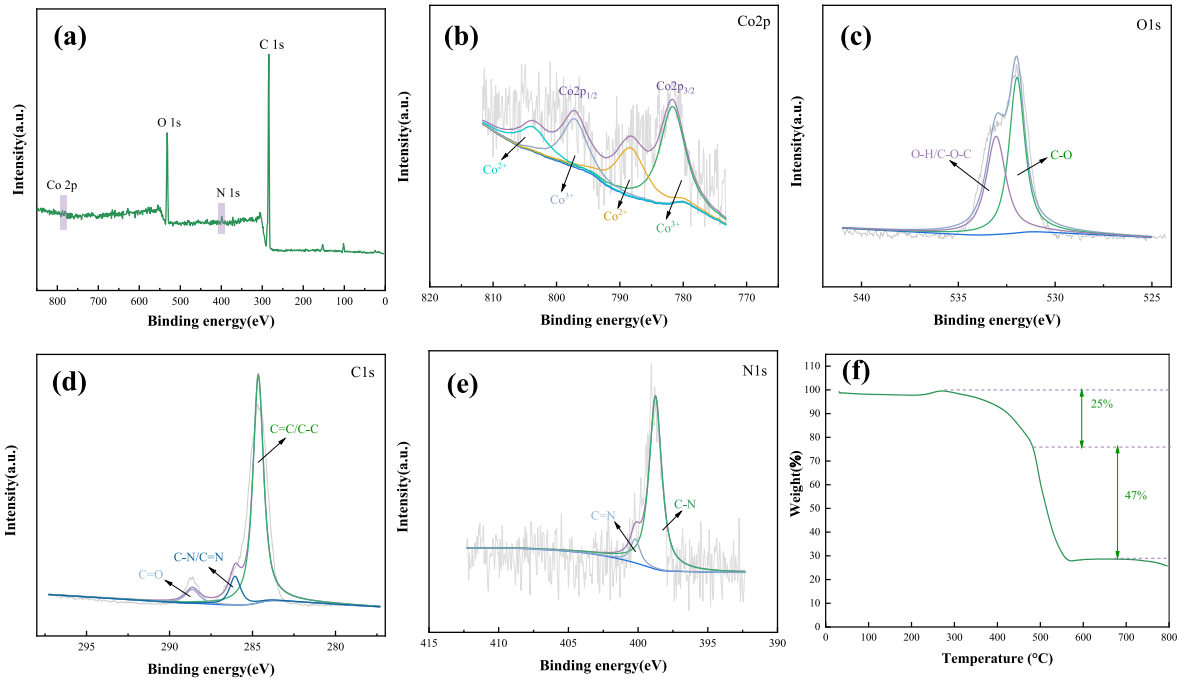

Fig. 4. XPS spectra of ZIF-67 before and after the reaction(a) survey of ZIF-67; (b) Co2p; (c) O1s; (d) C1s; (e) N1s; (f) TGA curve of ZIF-67.

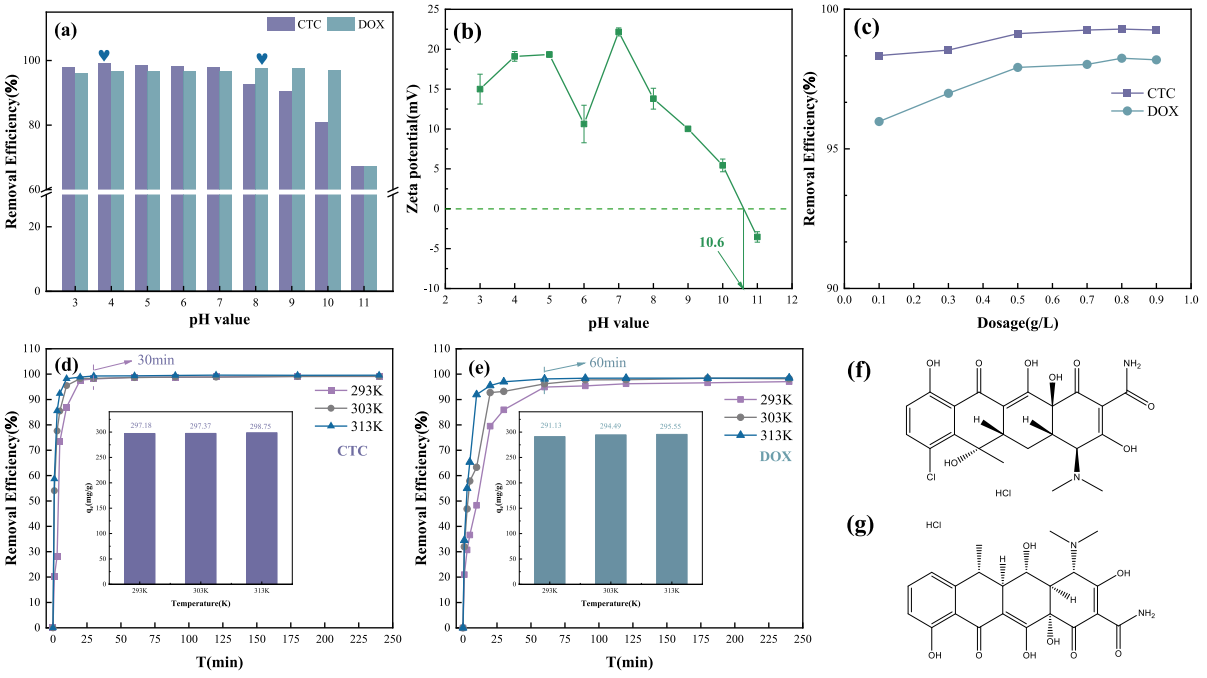

Fig. 5. (a) The removal efficiency of CTC and DOX in different pH, (b) the zeta potential of ZIF-67, (c) the removal efficiency of CTC and DOX in different dosage, (d–e) the removal efficiency and equilibrium adsorption capacity different temperature of CTC and DOX, (f) and (g) the structural formula of CTC and DOX.

3.2.3. Effects of temperature and contact time

Fig. 5(d and e) shows the removal efficiency of 150 mg/L of CTC and DOX at 293K, 303K, and 313K. When the reaction temperature increases, the adsorption efficiency also increases at the same time, and the time to reach the equilibrium is shortened. The final equilibrium removal rate also increases. The final equilibrium removal rate of CTC increased from 99.06 % (297.18 mg/g) to 99.58 % (298.75 mg/g), and the removal rate of DOX increased from 97.04 % (291.13 mg/g) to 98.5 % (295.55 mg/g). The time for CTC to reach equilibrium is shorter than that for DOX. Under the condition of 303K, the removal rate of ZIF-67 for CTC reached 98.34 % at the beginning of 30min, while the removal efficiency for DOX reached 96.17 % at the beginning of 60min. This also shows that the prepared adsorbent not only has a high removal efficiency of both CTC and DOX antibiotics, but also shows that the material can remove pollutants quickly. The adsorption reaction of CTC and DOX on ZIF-67 is an endothermic reaction.

3.3. Adsorption kinetics

Before the adsorption kinetics experiment, the experimental parameters were optimally selected, and the kinetic adsorption experiment was carried out at 303K and 0.5 g/L. The changes of adsorption capacity of ZIF-67 at the initial concentration of CTC and DOX are shown in Fig. 6. With the concentration increasing from 100 to 200 mg/L, the adsorption capacity of CTC and DOX increased from 198.55 to 397.18 mg/g and 196.94 to 394.89 mg/g, respectively. Among them, the adsorption removal rate of the two antibiotics was above 95 %. It can also be observed from Fig. 6 that antibiotics with lower concentrations take less time to reach equilibrium. The adsorption rate experiences a rapid ascent within the initial 30 min, attributed to the pollutant molecules occupying the plentiful active sites on the adsorbent [68,69]. The rate moderates between 30 and 60 min as the reduction in available active sites slows the adsorption rate, with equilibrium nearly reached thereafter.

In order to further explore the adsorption process of antibiotic pollutant molecules on adsorbents, three classical models were used to fit the experimental data, namely the pseudo-first-order model, the pseudo-second-order model and the intra-particle diffusion model. The fitting image is shown in Fig. 6, and the fitting parameters are summarized in Table 2. The equations for the three models are as follows Eqs. (3)–(5), respectively [58,70]:

$$q_t = q_e\left(1 - e^{-k_1 t}\right) \tag{3}$$

$$q_t = \frac{k_2 {q_e}^2 t}{1 + k_2 q_e t} \tag{4}$$

$$q_t = k_i t^{\frac{1}{2}} + C_i \tag{5}$$

where q_e (mg/g) is the adsorption capacity of CTC and DOX at the equilibrium time; q_t (mg/g) is the adsorption capacity of CTC and DOX at the time t (min); k_1 (min^{-1}) and k_2 (g mg^{-1} min^{-1}) are the constants of the pseudo-first-order model and pseudo-second-order

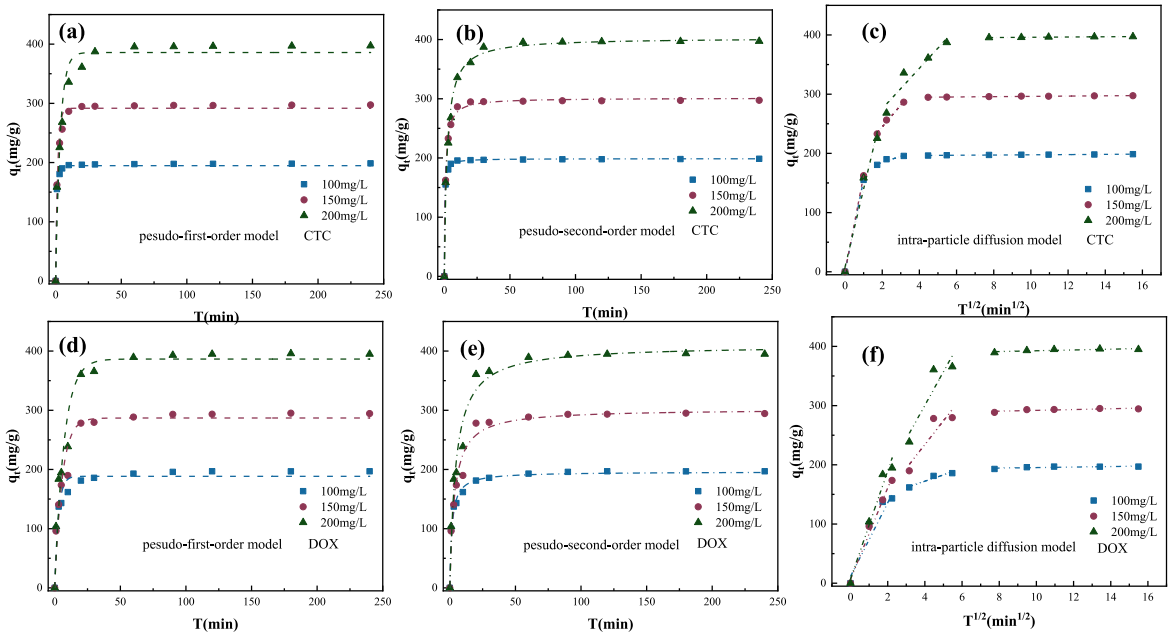

Fig. 6. The data fit curves on the adsorption kinetic models of (a–c) CTC, (d–f) DOX.

Table 2
Fitting parameters of the pseudo-first-order model and the pseudo-second-order model.

Model	Parameters	CTC			DOX		
		100 mg/L	150 mg/L	200 mg/L	100 mg/L	150 mg/L	200 mg/L
	$q_{e,exp}$	198.55	297.37	397.18	196.94	294.48	394.89
pseudo-first-order mode	q_e	194.78	291.70	385.89	188.48	286.92	386.56
	k_1	1.054	0.648	0.288	0.361	0.180	0.141
	R^2	0.974	0.981	0.963	0.934	0.948	0.957
pseudo-second-order model	q_e	198.88	301.37	403.12	196.16	302.22	409.99
	k_2	0.017	0.0039	0.0012	0.003	$9.6*10^{-4}$	$5.4*10^{-4}$
	R^2	0.999	0.998	0.992	0.982	0.976	0.978

model, respectively. k_i (mg (g $min^{1/2})^{-1}$) is the rate constant of intra-particle diffusion model; C_i (mg g^{-1}) is a constant related to the thickness of boundary layer in intra-particle diffusion model.

Noticeably, according to the R^2 results of the fitting results, the pseudo-second-order kinetic model can better describe the adsorption process of CTC and DOX on ZIF-67, which means that chemisorption dominates the adsorption process [71,72]. The intra-particle diffusion model is used to further understand the rate-controlling processes involved, it can be observed from Fig. 6 (c) and (f) that the entire adsorption process can be divided into three stages. The first stage is the rapid adsorption stage boundary layer diffusion, which is due to the diffusion of CTC and DOX from the solution to the surface of ZIF-67. The second stage is slower membrane diffusion, where CTC and DOX molecules are diffused from the outer surface to inner pore and capillary structure of ZIF-67. And the third stage is the final adsorption equilibrium stage [5,73]. In addition, the fitted curve does not pass through the origin, indicating that intraparticle diffusion is not the only rate-limiting step [58].

3.4. Adsorption isotherms and thermodynamic

To understand the impact of varying initial concentrations (100–1300 mg/L) of CTC and DOX on adsorption behaviors, the Freundlich, Langmuir, Temkin, and Sips models were applied to fit the experimental data, represented by Eqs. (6)–(9) respectively [1, 59,70]:

Freundlich model:

$$q_e = K_F C_e^{1/n} \tag{6}$$

where q_e (mg/g) is the equilibrium adsorption capacity of CTC and DOX; q_m (mg/g) is the maximum adsorption capacity; C_e (mg/L) is the equilibrium concentration of CTC and DOX; n is the heterogeneity factor; K_F ($mg^{1\text{-}1/n}\ L^{1/n}\ g^{-1}$) is the Freundlich constant related to the adsorption capacity.

Langmuir model:

$$q_e = \frac{q_m K_L C_e}{1 + K_L C_e} \tag{7}$$

where K_L (L/mg) is the adsorption equilibrium constant of Langmuir model.

Temkin model:

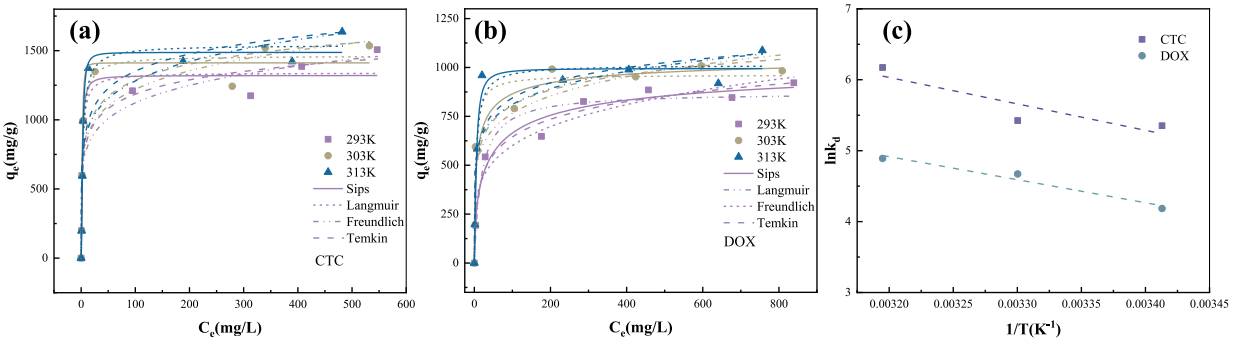

Fig. 7. The data fit the curve to the isotherm model of (a) CTC; (b) DOX; (c) Van't Hoff plot.

$$q_e = \frac{RT}{b_T}\ln(a_T C_e) \tag{8}$$

where a_T is the equilibrium binding constant related to the maximum binding energy; b_T is the Temkin constant connected with the heat of adsorption (kJ·mol^{-1}); R is the gas constant (8.314 × 10^{-3} kJ mol^{-1} K^{-1}); T is the temperature (K).

Sips model:

$$q_e = \frac{q_m a_s C_e^{1/n}}{1 + a_s C_e^{1/n}} \tag{9}$$

where a_s is the Sips constant related to the energy of adsorption; *1/n* is the constant related to the behavior of adsorption.

The fitting results are shown in Fig. 7(a and b), and the fitting parameters are shown in Table 3. At 293K, 303K and 313K, the adsorption amount increases with the increase of temperature, indicating that the increase of temperature is conducive to the reaction, indicating that the reaction is endothermic.

The Langmuir model posits that the adsorbent surface is covered by a single layer of adsorption, with no interaction between the adsorbent molecules. Conversely, the Freundlich model is better suited for describing the adsorption process in heterogeneous systems [12]. According to the R^2 value of the fitting results, the Sips model provides a more precise representation of the adsorption process of CTC and DOX on ZIF-67, indicating that the adsorption process of CTC and DOX on ZIF-67 is a complex adsorption process, including both monolayer adsorption at uniform binding sites and adsorption on heterogeneous surfaces [74]. Among them, Sips model fitted the maximum adsorption capacity of CTC and DOX to 1411.68 mg/g and 1073.28 mg/g at 303K, respectively. Higher than others that have been reported, summarized in Table 4. Temkin model has excellent fitting results for the adsorption process, with R^2 above 0.87, which indicates that the chemisorption exists between ZIF-67 and CTC and DOX molecules, but the low b_T (below 0.025) values in the fitting parameters indicate that chemical interaction is not the only adsorption mechanism [70,75].

In order to explore the thermodynamic properties of the adsorption process, thermodynamic parameters were explored at the temperature of 293K, 303K and 313K, and the thermodynamic parameters were calculated by Eqs. (10)–(12), respectively [33,76].

$$\Delta G^0 = -RT\ln k_d \tag{10}$$

$$k_d = \frac{q_e}{C_e} \tag{11}$$

$$\ln k_d = \frac{\Delta S^0}{R} - \frac{\Delta H^0}{RT} \tag{12}$$

where k_d is the distribution coefficient of thermodynamic at equilibrium; R is the gas constant (8.314 × 10^{-3} kJ mol^{-1} K^{-1}); T is the temperature (K).

The fitting results are shown in Table 5 and Fig. 7 (c). With the increase of temperature, the adsorption capacity of ZIF-67 for CTC and DOX also increased. As can be seen from Table 4. $\Delta G < 0$, that is the adsorption of CTC and DOX is spontaneous. $\Delta H > 0$ indicates that the reaction is endothermic. In addition, $\Delta S > 0$ indicates that the solid/liquid surface randomness increases during endothermic reaction [33].

3.5. The influence of co-existing ions

In practical applications, wastewater contains a variety of substances, necessitating an investigation into the effects of typical ions on the adsorption efficacy of ZIF-67 towards CTC and DOX. The effects of different cations and anions on the adsorption were

Table 3
Parameters of the isotherm models.

Model	Parameters	CTC			DOX		
		293K	303K	313K	293K	303K	313K
Sips	q_m	1320.56	1411.68	1487.44	1059.22	1073.28	995.12
	a_s	0.43	0.16	0.14	0.125	0.33	0.09
	n	0.73	0.43	0.54	1.77	1.82	0.70
	R^2	0.965	0.974	0.984	0.978	0.928	0.973
Freundlich	K_F	552.03	612.26	638.22	222.36	369.35	432.84
	n	6.49	6.67	6.61	4.63	6.32	7.33
	R^2	0.896	0.834	0.829	0.961	0.907	0.843
Langmuir	q_m	1340.41	1463.25	1541.38	872.25	962.55	1012.76
	K_L	0.495	0.37	0.32	0.054	0.258	0.20
	R^2	0.959	0.943	0.961	0.964	0.925	0.962
Temkin	a_T	27.29	21.65	18.59	1.41	12.94	18.42
	b_T	0.016	0.015	0.014	0.019	0.022	0.022
	R^2	0.923	0.871	0.873	0.981	0.923	0.880

Table 4
Comparison of the adsorption capacity of other adsorbents.

Adsorbents	Adsorbate	q_e (mg/g)	References
MWCNT/NH_2-MIL-53(Fe)	CTC	254.04	[5]
graphene oxide-γ-cyclodextrin nanocomposite	CTC	400.00	[10]
JLUE-MOG-Fe/Y	CTC	584.83	[77]
ZIF-67	CTC	1411.68	This work
Zr-MOFs	DOX	148.7	[78]
Cu-ZIF-8	DOX	379.2	[79]
LXR-BT	DOX	438.75	[80]
HEC-GO/Fe-Zn	DOX	16.5	[81]
ZIF-67	DOX	1073.28	This work

Table 5
Thermodynamic model parameters of CTC and DOX.

Parameters	CTC			DOX		
	293K	303K	313K	293K	303K	313K
ΔG (KJ mol^{-1})	−13.04	−13.66	−16.06	−10.19	−11.77	−12.72
ΔH (KJ mol^{-1})	30.98			27.01		
ΔS (J mol^{-1} K^{-1})	149.32			127.29		

investigated. In the experiment, cationic chloride salt and anionic sodium salt were used to investigate the anti-interference ability of ZIF-67. At an ion concentration of 20 mM, the adsorption results of CTC and DOX by Na^+, K^+, Al^{3+}, and Cl^-, NO_3^-, SO_4^{2-}, CO_3^{2-}, PO_4^{3-} ions on ZIF-67 are shown in Fig. 8(a) and (b). It can be seen from the figure that at the antibiotic concentration of 150 mg/L, the added Na^+, K^+, Cl^-, NO_3^-, SO_4^{2-} ion did not markedly alter the adsorption capacity, suggesting minimal interference from these ions in the reaction process. However, Al^{3+}, CO_3^{2-} and PO_4^{3-} exhibited varying degrees of adsorption inhibition.Notably, it can be clearly observed from Fig. 8(a and b) that Al^{3+} ion has a significant inhibitory effect on the adsorption of CTC and DOX, which may be attributed to the fact that Al^{3+} ion has a larger hydration radius and occupies more adsorption sites, which can inhibit the adsorption behavior of CTC and DOX on ZIF-67 [6]. For the co-existing anions, CO_3^{2-} and PO_4^{3-} have obvious inhibition on the adsorption behavior. CO_3^{2-} and PO_4^{3-} will change the pH of the solution, which is not conducive to the adsorption reaction. The influence of coexisting ions on adsorption behavior may be attributed to limited competition for active sites and changes in solution pH [60]. In summary, ZIF-67 also shows excellent adsorption capacity in the presence of coexisting ions, underscoring its potential as an effective adsorbent.

3.6. Reusability of ZIF-67

In economic and environmental considerations, the reusability of the adsorbent is a crucial condition. The experiment was carried out under the condition of three experiments (Fig. 8(c)). It can be easily observed from the figure that under the condition of three cycles, the adsorbent still maintains a high adsorption efficiency. The adsorption efficiency of ZIF-67 for CTC decreased from 99.16 % to 98.53 %, while the adsorption efficiency of DOX decreased from 97.61 % to 93.73 %. The results show that the adsorbent has good recyclability and is a promising adsorbent.

4. Conclusion

In summary, ZIF-67 nanoparticles were successfully synthesized at room temperature and under green condition. And the prepared materials were characterized by SEM, TEM, FT-IR, BET, XPS and TGA. This study extensively investigated the adsorption properties of CTC and DOX, examining the effects of various factors like solution pH, adsorbent dosage, temperature, initial concentration, contact time, and coexisting ions on their adsorption behaviors. The experimental results were fitted by adsorption kinetics model and adsorption isothermal model. The pseudo-second-order kinetics model and Sips model were shown by R^2 to be able to describe the adsorption process better. Model fitting indicates that the adsorption process is controlled by chemisorption, and the adsorption process on ZIF-67 is complex. At 303K, the maximum adsorption capacity of CTC and DOX on ZIF-67 was 1411.68 and 1073.28 mg/g, respectively. And the high adsorption capacity of ZIF-67 for antibiotics is attributed to the specific surface area and abundant active sites of the adsorbent. In addition, the characterization results of after reaction show that the main mechanism of adsorption process is mainly pore filling, electrostatic interaction and π-π interaction. After three adsorption experiments, ZIF-67 still maintained high removal rates (98.53 % and 93.73 %) of CTC and DOX. Therefore, the prepared adsorbents may have tremendous application prospects in the direction of removing these two antibiotics.

Conflicts of interest statement

There is no conflict of interest to declare.

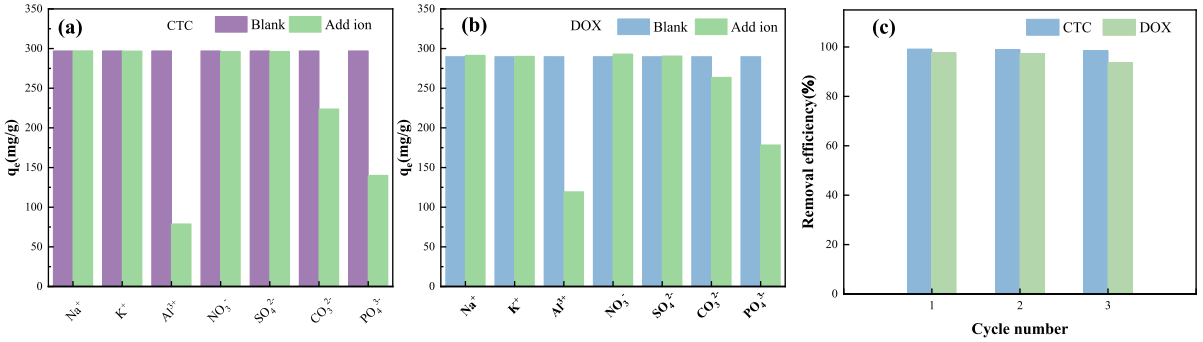

Fig. 8. Effects of coexisting ions on (a) CTC and (b) DOX; (c) removal efficiency of ZIF-67 after circulation.

Data availability statement

The original contributions presented in this study are included in the article. No data were deposited in any publicly available repositories. Further inquiries can be directed to the corresponding authors.

CRediT authorship contribution statement

Ke Li: Writing – original draft, Methodology. **Miaomiao Chen:** Writing – original draft, Investigation. **Lei Chen:** Writing – review & editing, Supervision, Resources, Project administration, Funding acquisition. **Songying Zhao:** Data curation. **Wenbo Pan:** Investigation, Formal analysis. **Pan Li:** Investigation, Data curation.

Declaration of competing interest

The authors declare that they have no known competing financial interests or personal relationships that could have appeared to influence the work reported in this paper.

Acknowledgments

This research was funded by Jilin Province Outstanding Young and Middle-aged Talent (Team) Program for Scientific and Technological Innovation and Entrepreneurship (20240601029RC). All authors thank the editor and anonymous reviewers for their constructive comments and suggestions to improve the quality of this paper.

References

[1] G.Y. Chen, S. He, G.B. Shi, Y.S. Ma, C.C. Ruan, X. Jin, Q.L. Chen, X.Y. Liu, H.M. Dai, X.F. Chen, D.M. Huang, In-situ immobilization of ZIF-67 on wood aerogel for effective removal of tetracycline from water, Chem. Eng. J. 423 (2021), https://doi.org/10.1016/j.cej.2021.130184.
[2] A. Pollap, J. Kochana, Electrochemical immunosensors for antibiotic detection, Biosensors 9 (2) (2019), https://doi.org/10.3390/bios9020061.
[3] C.Y. Du, Z. Zhang, G.L. Yu, H.P. Wu, H. Chen, L. Zhou, Y. Zhang, Y.H. Su, S.Y. Tan, L. Yang, J.H. Song, S.T. Wang, A review of metal organic framework (MOFs)-based materials for antibiotics removal via adsorption and photocatalysis, Chemosphere 272 (2021), https://doi.org/10.1016/j.chemosphere.2020.129501.
[4] M.H. Kabir, M.S. Hossain, M.M. Rahman, M. Ashrafuzzaman, M. Hasan, M.Y. Pabel, D. Islam, M. Shahriar Bashar, T. Faruque, S. Yasmin, Green reduction of waste-battery-derived graphene oxide by jute leaves and its application for the removal of tetracyclines from aqueous media, ACS Sustainable Resource Management (2024), https://doi.org/10.1021/acssusresmgt.4c00181.
[5] W.P. Xiong, Z.T. Zeng, X. Li, G.M. Zeng, R. Xiao, Z.H. Yang, Y.Y. Zhou, C. Zhang, M. Cheng, L. Hu, C.Y. Zhou, L. Qin, R. Xu, Y.R. Zhang, Multi-walled carbon nanotube/amino-functionalized MIL-53(Fe) composites: remarkable adsorptive removal of antibiotics from aqueous solutions, Chemosphere 210 (2018) 1061–1069, https://doi.org/10.1016/j.chemosphere.2018.07.084.
[6] J.H. Zhou, F. Ma, H.J. Guo, Adsorption behavior of tetracycline from aqueous solution on ferroferric oxide nanoparticles assisted powdered activated carbon, Chem. Eng. J. 384 (2020), https://doi.org/10.1016/j.cej.2019.123290.
[7] S.N. Zhang, J.H. Wang, Removal of chlortetracycline from water by *Bacillus cereus* immobilized on Chinese medicine residues biochar, Environ. Technol. Innovat. 24 (2021), https://doi.org/10.1016/j.eti.2021.101930.
[8] S. Liu, W.H. Xu, Y.G. Liu, X.F. Tan, G.M. Zeng, X. Li, J. Liang, Z. Zhou, Z.L. Yan, X.X. Cai, Facile synthesis of Cu(II) impregnated biochar with enhanced adsorption activity for the removal of doxycycline hydrochloride from water, Sci. Total Environ. 592 (2017) 546–553, https://doi.org/10.1016/j.scitotenv.2017.03.087.
[9] A.C. Shanoy, S. Subbiah, A. Gentles, D. Oliver, P. Stonum, T.A. Brooks, E.E. Smith, Qualitative and quantitative drug residue analyses: chlortetracycline in white-tailed deer (*Odocoileus virginianus*) and supermarket meat by liquid chromatography tandem-mass spectrometry, J. Chromatogr. B 1092 (2018) 237–243, https://doi.org/10.1016/j.jchromb.2018.05.027.
[10] Z.A. Alothman, N. AlMasoud, X.Y. Mbianda, I. Ali, Synthesis and characterization of γ-cyclodextrin-graphene oxide nanocomposite: sorption, kinetics, thermodynamics and simulation studies of tetracycline and chlortetracycline antibiotics removal in water, J. Mol. Liq. 345 (2022), https://doi.org/10.1016/j.molliq.2021.116993.
[11] G. Kaur, N. Singh, A. Rajor, Efficient adsorption of doxycycline hydrochloride using deep eutectic solvent functionalized activated carbon derived from pumpkin seed shell, ChemistrySelect 6 (13) (2021) 3139–3150, https://doi.org/10.1002/slct.202100182.

[12] J. Xia, Y.X. Gao, G. Yu, Tetracycline removal from aqueous solution using zirconium-based metal-organic frameworks (Zr-MOFs) with different pore size and topology: adsorption isotherm, kinetic and mechanism studies, J. Colloid Interface Sci. 590 (2021) 495–505, https://doi.org/10.1016/j.jcis.2021.01.046.

[13] O. Moradi, I.D. Sharabaf, Separation of organic contaminant (dye) using the modified porous metal-organic framework (MIL), Environ. Res. 214 (2022), https://doi.org/10.1016/j.envres.2022.114006.

[14] O. Moradi, S. Panahandeh, Fabrication of different adsorbents based on zirconium oxide, graphene oxide, and dextrin for removal of green malachite dye from aqueous solutions, Environ. Res. 214 (2022), https://doi.org/10.1016/j.envres.2022.114042.

[15] A. Mazinai, K. Zare, O. Moradi, H. Attar, Sulfonated calixarene modified Poly(methyl methacrylate) nanoparticles:A promising adsorbent for Removal of Vanadium Ions from aqueous media, Chemosphere 299 (2022), https://doi.org/10.1016/j.chemosphere.2022.134459.

[16] M. SefidSiahbandi, O. Moradi, B. Akbari-adergani, P.A. Azar, M.S. Tehrani, Fabrication and implementation of bimetallic Fe/Zn nanoparticles (mole ratio 1:1) loading on hydroxyethylcellulose - graphene oxide for removal of tetracycline antibiotic from aqueous solution, Chemosphere 312 (2023), https://doi.org/10.1016/j.chemosphere.2022.137184.

[17] H.A. Yurtsever, A.E. Cetin, Fabrication of ZIF-8 decorated copper doped TiO_2 nanocomposite at low ZIF-8 loading for solar energy applications, Colloids Surf. Physicochem. Eng. Aspects 625 (2021), https://doi.org/10.1016/j.colsurfa.2021.126980.

[18] S.M. Samianifard, M. Kalaee, O. Moradi, N.M. Mahmoodi, D. Zaarei, Novel biocomposite (Starch/metal-organic framework/Graphene oxide): synthesis, characterization and visible light assisted dye degradation, J. Photochem. Photobiol. Chem. 450 (2024), https://doi.org/10.1016/j.jphotochem.2023.115417.

[19] B. Farahani, M. Giahi, M.H. Ghorbani, R. Fazaeli, O. Moradi, Synthesis of CuS/NiS heterostructural photocatalyst and its performance in the degradation of metronidazole and diclofenac drugs: optimization of operating conditions, Journal of Nanostructure in Chemistry 13 (2) (2023) 303–320, https://doi.org/10.1007/s40097-022-00520-2.

[20] O. Moradi, H. Alizadeh, S. Sedaghat, Handling Editor: derek Muir Keywords: maltodextrin/reduced graphene/copper oxide nanoparticles (II) nanocomposite Removal of pharmaceutical Diclofenac and amoxicillin, Chemosphere 299 (2022), https://doi.org/10.1016/j.chemosphere.2022.134435.

[21] S. Yasmin, M.G. Azam, M.S. Hossain, U.S. Akhtar, M.H. Kabir, Efficient removal of ciprofloxacin from aqueous solution using Zn–C battery derived graphene oxide enhanced by hydrogen bonding, electrostatic and π-π interaction, Heliyon 10 (12) (2024) e33317, https://doi.org/10.1016/j.heliyon.2024.e33317.

[22] D. Pang, Y. Liu, H.O. Song, D.Z. Chen, W.Q. Zhu, R.M. Liu, H. Yang, A.M. Li, S.P. Zhang, Trace Ti^{3+}- and N-codoped TiO_2 nanotube array anode for significantly enhanced electrocatalytic degradation of tetracycline and metronidazole, Chem. Eng. J. 405 (2021), https://doi.org/10.1016/j.cej.2020.126982.

[23] Z. Zeng, P. Zheng, D. Kang, W.J. Li, D.D. Xu, W.D. Chen, C. Pan, L.Y. Guo, The removal of veterinary antibiotics in the high-rate anaerobic bioreactor: continuous and batch studies, Water Sci. Technol. 86 (7) (2022) 1668–1680, https://doi.org/10.2166/wst.2022.293.

[24] M.S. Hossain, M.H. Kabir, M.A. Ali Shaikh, M.A. Haque, S. Yasmin, Ultrafast and simultaneous removal of four tetracyclines from aqueous solutions using waste material-derived graphene oxide-supported cobalt–iron magnetic nanocomposites, RSC Adv. 14 (2) (2024) 1431–1444, https://doi.org/10.1039/D3RA07597D.

[25] M.H. Khan, H.S. Jung, W. Lee, J.Y. Jung, Chlortetracycline degradation by photocatalytic ozonation in the aqueous phase: mineralization and the effects on biodegradability, Environ. Technol. 34 (4) (2013) 495–502, https://doi.org/10.1080/09593330.2012.701332.

[26] F.B. Yin, S.Y. Lin, X.Q. Zhou, H.M. Dong, Y.H. Zhan, Fate of antibiotics during membrane separation followed by physical-chemical treatment processes, Sci. Total Environ. 759 (2021), https://doi.org/10.1016/j.scitotenv.2020.143520.

[27] M.B. Ahmed, J.L. Zhou, H.H. Ngo, W.S. Guo, Adsorptive removal of antibiotics from water and wastewater: progress and challenges, Sci. Total Environ. 532 (2015) 112–126, https://doi.org/10.1016/j.scitotenv.2015.05.130.

[28] X. Chen, X. Jiang, C.J. Yin, B.L. Zhang, Q.Y. Zhang, Facile fabrication of hierarchical porous ZIF-8 for enhanced adsorption of antibiotics, J. Hazard Mater. 367 (2019) 194–204, https://doi.org/10.1016/j.jhazmat.2018.12.080.

[29] S.A.R. Ahmadi, M.R. Kalaee, O. Moradi, F. Nosratinia, M. Abdouss, Core-shell activated carbon-ZIF-8 nanomaterials for the removal of tetracycline from polluted aqueous solution, Adv. Compos. Hybrid Mater. 4 (4) (2021) 1384–1397, https://doi.org/10.1007/s42114-021-00357-3.

[30] O. Moradi, A. Pudineh, S. Sedaghat, Synthesis and characterization Agar/GO/ZnO NPs nanocomposite for removal of methylene blue and methyl orange as azo dyes from food industrial effluents, Food Chem. Toxicol. 169 (2022), https://doi.org/10.1016/j.fct.2022.113412.

[31] O. Moradi, M.A. Madanpisheh, M. Moghaddas, Synthesis of GO/HEMA, GO/HEMA/TiO_2, and GO/Fe_3O_4/HEMA as novel nanocomposites and their dye removal ability, Adv. Compos. Hybrid Mater. 4 (4) (2021) 1185–1204, https://doi.org/10.1007/s42114-021-00353-7.

[32] O. Moradi, A review on nanomaterial-based electrochemical sensors for determination of vanillin in food samples, Food Chem. Toxicol. 168 (2022), https://doi.org/10.1016/j.fct.2022.113391.

[33] R. Zhao, T. Ma, S. Zhao, H. Rong, Y. Tian, G. Zhu, Uniform and stable immobilization of metal-organic frameworks into chitosan matrix for enhanced tetracycline removal from water, Chem. Eng. J. 382 (2020), https://doi.org/10.1016/j.cej.2019.122893.

[34] X.B. Zhang, W.S. Guo, H.H. Ngo, H.T. Wen, N. Li, W. Wu, Performance evaluation of powdered activated carbon for removing 28 types of antibiotics from water, J. Environ. Manag. 172 (2016) 193–200, https://doi.org/10.1016/j.jenvman.2016.02.038.

[35] T.Y. Wang, X. Pan, W.W. Ben, J.B. Wang, P. Hou, Z.M. Qiang, Adsorptive removal of antibiotics from water using magnetic ion exchange resin, J. Environ. Sci. 52 (2017) 111–117, https://doi.org/10.1016/j.jes.2016.03.017.

[36] J.S. Gao, J.J. Chen, X.N. Li, M.W. Wang, X.Y. Zhang, F. Tan, S.T. Xu, J. Liu, Azide-functionalized hollow silica nanospheres for removal of antibiotics, J. Colloid Interface Sci. 444 (2015) 38–41, https://doi.org/10.1016/j.jcis.2014.12.054.

[37] D. Hao, Y. Chen, Y. Zhang, N. You, Nanocomposites of zero-valent iron@biochar derived from agricultural wastes for adsorptive removal of tetracyclines, Chemosphere 284 (2021), https://doi.org/10.1016/j.chemosphere.2021.131342.

[38] A.O. Egbedina, C.G. Ugwuja, P.A. Dare, H.D. Sulaiman, B.I. Olu-Owolabi, K.O. Adebowale, CTAB-Activated carbon from Peanut Husks for the removal of antibiotics and antibiotic-resistant bacteria from water, Environmental Processes 10 (2) (2023), https://doi.org/10.1007/s40710-023-00636-9.

[39] L. Joseph, B.M. Jun, M. Jang, C.M. Park, J.C. Muñoz-Senmache, A.J. Hernández-Maldonado, A. Heyden, M. Yu, Y. Yoon, Removal of contaminants of emerging concern by metal-organic framework nanoadsorbents: a review, Chem. Eng. J. 369 (2019) 928–946, https://doi.org/10.1016/j.cej.2019.03.173.

[40] A.F. Sahayaraj, H.J. Prabu, J. Maniraj, M. Kannan, M. Bharathi, P. Diwahar, J. Salamon, Metal-organic frameworks (MOFs): the next generation of materials for catalysis, gas storage, and separation, J. Inorg. Organomet. Polym. Mater. 33 (7) (2023) 1757–1781, https://doi.org/10.1007/s10904-023-02657-1.

[41] J. Khodayari, K. Zare, O. Moradi, M. Kalaee, N.M. Mahmoodi, Synthesis of eco-friendly carboxymethyl cellulose/metal-organic framework biocomposite and its photocatalytic activity, J. Photochem. Photobiol. Chem. 446 (2024), https://doi.org/10.1016/j.jphotochem.2023.115097.

[42] O. Moradi, Electrochemical sensors based on carbon nanostructures for the analysis of bisphenol A-A review, Food Chem. Toxicol. 165 (2022), https://doi.org/10.1016/j.fct.2022.113074.

[43] Z.B. Yang, D.D. Li, D. Ao, C. Ma, N. Li, Y.X. Sun, Z.H. Qiao, C.L. Zhong, M.D. Guiver, Self-supported membranes fabricated by a polymer-hydrogen bonded network with a rigidified MOF framework, J. Membr. Sci. 650 (2022), https://doi.org/10.1016/j.memsci.2022.120427.

[44] J. Tang, C.Y. Huang, Y.Q. Liu, T.Q. Wang, M. Yu, H.S. Hao, W.W. Zeng, W.X. Huang, J.Q. Wang, M.Y. Wu, Metal-organic framework nanoshell structures: preparation and biomedical applications, Coord. Chem. Rev. 490 (2023), https://doi.org/10.1016/j.ccr.2023.215211.

[45] O. Moradi, G. Sharma, Emerging novel polymeric adsorbents for removing dyes from wastewater: a comprehensive review and comparison with other adsorbents, Environ. Res. 201 (2021), https://doi.org/10.1016/j.envres.2021.111534.

[46] C.L. Pu, H.L. Zhao, Y.Y. Hong, Q.L. Zhan, M.B. Lan, Facile preparation of hydrophilic mesoporous metal-organic framework via synergistic etching and surface functionalization for glycopeptides analysis, Anal. Chem. 92 (2) (2020) 1940–1947, https://doi.org/10.1021/acs.analchem.9b04236.

[47] K.Y.A. Lin, H.A. Chang, Ultra-high adsorption capacity of zeolitic imidazole framework-67 (ZIF-67) for removal of malachite green from water, Chemosphere 139 (2015) 624–631, https://doi.org/10.1016/j.chemosphere.2015.01.041.

[48] J.F. Qian, F.A. Sun, L.Z. Qin, Hydrothermal synthesis of zeolitic imidazolate framework-67 (ZIF-67) nanocrystals, Mater. Lett. 82 (2012) 220–223, https://doi.org/10.1016/j.matlet.2012.05.077.

[49] J. Dai, C.X. Li, S.Z. Xiao, J. Liu, J. He, J.D. Li, L.Y. Wang, J.D. Lei, Fabrication of novel ZIF-67 composite microspheres for effective adsorption and solid-phase extraction of dyes from water, ChemistrySelect 3 (21) (2018) 5833–5842, https://doi.org/10.1002/slct.201800778.

[50] M.A. Nazir, M.S. Bashir, M. Jamshaid, A. Anum, T. Najam, K. Shahzad, M. Imran, S.S.A. Shah, A.U. Rehman, Synthesis of porous secondary metal-doped MOFs for removal of Rhodamine B from water: role of secondary metal on efficiency and kinetics, Surface. Interfac. 25 (2021), https://doi.org/10.1016/j.surfin.2021.101261.

[51] P. Dai, Y.C. Yao, E.Z. Hu, D.Y. Xu, Z.C. Li, C.S. Wang, Self-assembled ZIF-67@graphene oxide as a cobalt-based catalyst precursor with enhanced catalytic activity toward methanolysis of sodium borohydride, Appl. Surf. Sci. 546 (2021), https://doi.org/10.1016/j.apsusc.2021.149128.

[52] T.B. Nguyen, V.A. Thai, C.W. Chen, C.P. Huang, R.A. Doong, L.E. Chen, C.D. Dong, N-doping modified zeolitic imidazole Framework-67 (ZIF-67) for enhanced peroxymonosulfate activation to remove ciprofloxacin from aqueous solution, Sep. Purif. Technol. 288 (2022), https://doi.org/10.1016/j.seppur.2022.120719.

[53] K. Zhou, B. Mousavi, Z.X. Luo, S. Phatanasri, S. Chaemchuen, F. Verpoort, Characterization and properties of Zn/Co zeolitic imidazolate frameworks *vs.* ZIF-8 and ZIF-67, J. Mater. Chem. A 5 (3) (2017) 952–957, https://doi.org/10.1039/c6ta07860e.

[54] S. Saghir, Z.G. Xiao, Synthesis of novel Ag@ZIF-67 rhombic dodecahedron for enhanced adsorptive removal of antibiotic and organic dye, J. Mol. Liq. 328 (2021), https://doi.org/10.1016/j.molliq.2021.115323.

[55] M. Afkhami-Ardekani, M.R. Naimi-Jamal, S. Doaee, S. Rostamnia, Solvent-free mechanochemical preparation of metal-organic framework ZIF-67 impregnated by Pt nanoparticles for water purification, Catalysts 13 (1) (2023), https://doi.org/10.3390/catal13010009.

[56] Z. Naghshbandi, M. Gholinejad, J.M. Sansano, New recyclable Co-based trimetallic zeolite imidazolate framework (Cu-Ni@ZIF-67) as an efficient catalyst for different reduction reactions, Polyhedron 243 (2023), https://doi.org/10.1016/j.poly.2023.116523.

[57] N. Garg, M. Kumar, N. Kumari, A. Deep, A.L. Sharma, Chemoresistive room-temperature sensing of ammonia using zeolite imidazole framework and reduced graphene oxide (ZIF-67/rGO) composite, ACS Omega 5 (42) (2020) 27492–27501, https://doi.org/10.1021/acsomega.0c03981.

[58] X. Hu, Y.J. Xie, R.N. He, L.X. Yao, S.S. Ma, C.H. Bai, Nano-iron wrapped by graphitic carbon in the carbonaceous matrix for efficient removal of chlortetracycline, Sep. Purif. Technol. 279 (2021), https://doi.org/10.1016/j.seppur.2021.119693.

[59] Z. Wu, X. Wang, J. Qiu, C. Liu, Z. Yu, J. Zhang, Z. Qiu, In-situ uniform growth of ZIF-8 on 3D flower-like NiCoLDH microspheres to enhance tetracycline and doxycycline removal from wastewater: anti-interference and stability tests, Sep. Purif. Technol. 302 (2022), https://doi.org/10.1016/j.seppur.2022.122078.

[60] Y. Zhang, Z.J. Huang, X. Fang, Y.H. Chen, S.S. Fan, H.C. Xu, Preparation of magnetic porous biochar through hydrothermal pretreatment combined with K_2FeO_4 activation to improve tetracycline removal, Microporous Mesoporous Mater. 343 (2022), https://doi.org/10.1016/j.micromeso.2022.112188.

[61] J. Pan, L. Che, T. Wei, Y. Cong, S.-W. Lv, Introduction of ZIF-67 shell in $NiCo_2O_4$ nanocage to enhance peroxymonosulfate activation based on nonradical pathway for effective removal of organic contaminant, Appl. Surf. Sci. 637 (2023), https://doi.org/10.1016/j.apsusc.2023.157997.

[62] X. Wu, D.D. Sun, H.C. Ma, C. Ma, X.X. Zhang, J. Hao, Activation of peroxymonosulfate by magnetic CuFe2O4@ZIF-67 composite catalyst for the study on the degradation of methylene blue, Colloids Surf. Physicochem. Eng. Aspects 637 (2022), https://doi.org/10.1016/j.colsurfa.2022.128278.

[63] Z. Zhang, Y. Chen, C.Y. Hu, C. Zuo, P. Wang, W.Q. Chen, T.Q. Ao, Efficient removal of tetracycline by a hierarchically porous ZIF-8 metal organic framework, Environ. Res. 198 (2021), https://doi.org/10.1016/j.envres.2021.111254.

[64] Q.P. Fu, J. Lou, H. Yuan, R.B. Zhang, C.M. Zhang, C.L. Mo, J. Luo, L. Zha, P. Wu, In-situ grown ZIF-67@chitosan (ZIF-67@CS) for highly efficient removal of Pb (II) from water, J. Solid State Chem. 316 (2022), https://doi.org/10.1016/j.jssc.2022.123629.

[65] Y.L. Liu, W.W. Li, Y.B. Gao, J. Wang, G.H. Cheng, J.F. Chen, X. Li, G.F. Zhu, Highly efficient and rapid removal of non-steroidal anti-inflammatory drugs from environmental samples based on an eco-friendly ZIF-67-molecularly imprinted composite, Chem. Eng. J. 443 (2022), https://doi.org/10.1016/j.cej.2022.136396.

[66] Y. Yusran, D. Xu, Q.R. Fang, D.L. Zhang, S.L. Qiu, MOF-derived Co@N-C nanocatalyst for catalytic reduction of 4-nitrophenol to 4-aminophenol, Microporous Mesoporous Mater. 241 (2017) 346–354, https://doi.org/10.1016/j.micromeso.2016.12.029.

[67] M. Kasula, T. Le, A. Thomsen, M.R. Esfahani, Silver metal organic frameworks and copper metal organic frameworks immobilized on graphene oxide for enhanced adsorption in water treatment, Chem. Eng. J. 439 (2022), https://doi.org/10.1016/j.cej.2022.135542.

[68] M. Anari-Anaraki, A. Nezamzadeh-Ejhieh, Modification of an Iranian clinoptilolite nano-particles by hexadecyltrimethyl ammonium cationic surfactant and dithizone for removal of Pb(II) from aqueous solution, J. Colloid Interface Sci. 440 (2015) 272–281, https://doi.org/10.1016/j.jcis.2014.11.017.

[69] F. Mojumder, S. Yasmin, M.A.A. Shaikh, P. Chowdhury, M.H. Kabir, Synthesis of reusable graphene oxide based nickel-iron superparamagnetic nanoadsorbent from electronic waste for the removal of doxycycline in aqueous media, Journal of Hazardous Materials Advances 14 (2024) 100429, https://doi.org/10.1016/j.hazadv.2024.100429.

[70] F. Zhao, S. Fang, Y. Gao, J. Bi, Removal of aqueous pharmaceuticals by magnetically functionalized Zr-MOFs: adsorption Kinetics, Isotherms, and regeneration, J. Colloid Interface Sci. 615 (2022) 876–886, https://doi.org/10.1016/j.jcis.2022.02.018.

[71] X.L. Guo, L.J. Kong, Y. Ruan, Z.H. Diao, K.M. Shih, M.H. Su, L.A. Hou, D.Y. Chen, Green and facile synthesis of cobalt-based metal-organic frameworks for the efficient removal of Congo red from aqueous solution, J. Colloid Interface Sci. 578 (2020) 500–509, https://doi.org/10.1016/j.jcis.2020.05.126.

[72] J.Y. Liang, W.X. Zhang, X.W. Yao, M.L. Chen, X. Chen, L.J. Kong, Z.H. Diao, New insights into co-adsorption of Cr6+and chlortetracycline by a new fruit peel based biochar composite from water: behavior and mechanism, Colloids Surf. Physicochem. Eng. Aspects 672 (2023), https://doi.org/10.1016/j.colsurfa.2023.131764.

[73] S.Y. Fan, Y.F. Qu, L.X. Yao, J.H. Ren, R. Luque, Z.L. He, C.H. Bai, MOF-derived cluster-shaped magnetic nanocomposite with hierarchical pores as an efficient and regenerative adsorbent for chlortetracycline removal, J. Colloid Interface Sci. 586 (2021) 433–444, https://doi.org/10.1016/j.jcis.2020.10.107.

[74] H.X. Duan, X. Hu, Z.R. Sun, Magnetic zeolite imidazole framework material-8 as an effective and recyclable adsorbent for removal of ceftazidime from aqueous solution, J. Hazard Mater. 384 (2020), https://doi.org/10.1016/j.jhazmat.2019.121406.

[75] Z. Zhang, Y. Chen, P. Wang, Z. Wang, C. Zuo, W.Q. Chen, T.Q. Ao, Facile fabrication of N-doped hierarchical porous carbons derived from soft-templated ZIF-8 for enhanced adsorptive removal of tetracycline hydrochloride from water, J. Hazard Mater. 423 (2022), https://doi.org/10.1016/j.jhazmat.2021.127103.

[76] Y. Liu, Is the free energy change of adsorption correctly calculated? J. Chem. Eng. Data 54 (7) (2009) 1981–1985, https://doi.org/10.1021/je800661q.

[77] S. Xia, J.M. Sun, W.T. Sun, Bimetallic metal-organic gel for effective removal of chlortetracycline hydrochloride from aqueous solution:Adsorption isotherm, kinetic and mechanism studies, Colloids Surf. Physicochem. Eng. Aspects 649 (2022), https://doi.org/10.1016/j.colsurfa.2022.129403.

[78] Q. Ren, Y. Ma, F. Wei, L. Qin, H. Chen, Z. Liang, S. Wang, Preparation of Zr-MOFs for the adsorption of doxycycline hydrochloride from wastewater, Green Process. Synth. 12 (1) (2023), https://doi.org/10.1515/gps-2022-8127.

[79] J.L. Zhang, K.X. Liu, Enhanced adsorption of doxycycline hydrochloride (DCH) from water on zeolitic imidazolate framework-8 modified by Cu^{2+} (Cu-ZIF-8), water, Air, Soil Pollut. 231 (2) (2020), https://doi.org/10.1007/s11270-020-4455-8.

[80] Y. Kong, L. Wang, Y.Y. Ge, H.Y. Su, Z.L. Li, Lignin xanthate resin-bentonite clay composite as a highly effective and low-cost adsorbent for the removal of doxycycline hydrochloride antibiotic and mercury ions in water, J. Hazard Mater. 368 (2019) 33–41, https://doi.org/10.1016/j.jhazmat.2019.01.026.

[81] M. SefidSiahbandi, O. Moradi, B. Akbari-adergani, P.A. Azar, M.S. Tehrani, The effect of Fe-Zn mole ratio (2:1) bimetallic nanoparticles supported by hydroxyethyl cellulose/graphene oxide for high-efficiency removal of doxycycline, Environ. Res. 218 (2023), https://doi.org/10.1016/j.envres.2022.114925.